Implementing both short- and long-working-distance optical trappings into a commercial microscope

Pavel Kraikivski
Max Planck Institute of Colloids and Interfaces, Science Park Golm, 14424 Potsdam, Germany

Bernard Pouligny
Centre de recherche Paul-Pascal, Avenue Schweitzer, 33600 Pessac, France

Rumiana Dimova
Max Planck Institute of Colloids and Interfaces, Science Park Golm, 14424 Potsdam, Germany

(Received 23 May 2006; accepted 26 October 2006; published online 22 November 2006)

Optical tweezers are now a widespread tool based on three-dimensional trapping by a tightly focused single laser beam. This configuration only works with large numerical aperture and short-working-distance (SWD) objectives, restricting optical manipulation to the high magnification end of the microscope nosepiece. Certain applications of optical trapping demand long-working distances (LWDs) at moderate magnification, imposing a more complex two-beam trapping configuration. In this article, we describe a complete setup that incorporates both SWD and LWD optical trapping functionalities into a single Axiovert 200M Zeiss microscope. We evaluate the performance of the setup in both trapping modes with latex particles, either fluorescent or not, of different sizes, in the $1-20$ μm range. We provide practical information allowing for optimal configuration of the two-beam geometry, in relation with longitudinal and lateral stabilities of the trap. © *2006 American Institute of Physics.* [DOI: 10.1063/1.2400023]

I. INTRODUCTION

Early works on levitation and trapping of small objects by laser beams date back to the 1970s.[1–4] In this period, experiments were carried out with specialized setups, involving two or more intersecting beams,[1–4] to create a kind of electromagnetic box inside which a micrometer-sized particle could be held and trapped. Principles were set out and verified about the stability of trapping in such boxes as a function of particle characteristics.[1–4] The two-beam trap geometry, based on these principles, is fairly simple, as it only involves two coaxial counterpropagating beams. Both beams have small numerical apertures (e.g., ~0.1), and their foci must be separated by a small distance (denoted as Δ in Sec. IV) along the common axis, of the order of a diffraction length. The trapping region is located between the two foci.

After the pioneering works on laser induced radiation pressure (RP), the two-beam geometry was only used in a few cases for applications in biophysics and biology.[5–8] Much more widespread is the so-called "optical tweezer" geometry,[9] based on a single tightly focused beam. In comparison to the two-beam concept, the single-beam trap has the twofold advantage of simplicity and size independence; i.e., particles with sizes ranging from less than 1 μm up to about 20 μm can be trapped with the same setup, without any adjustment except that of the beam power.[10,11] Simplicity stems from the fact that the trap just needs a single collimated beam, directed through a microscope objective with a very large aperture. The laser beam must be expanded to be wide enough to cover the exit pupil of the objective. Because the optical setup can be built around a commercial microscope, with just a few optics to shape and direct the laser beam through a video or fluorescence port, the concept has become very popular and is now a standard tool added to the arsenal of optical microscopy techniques. Of course, a great variety of sophisticated versions involving scanning and multiple traps has been developed in the past 15 years (for a recent review, see Ref. 12), but the basic principles remain the same.

The single-beam trap, however, has limitations and drawbacks, all of them consequences of the requirement of a very large aperture objective. (i) Such objectives are of immersion type (most often in oil, sometimes in water) and have extremely short-working distances (WDs), between 0.1 and 0.2 mm. (ii) They are at the high magnification end (100× is standard) of the microscope nosepiece, providing a relatively narrow field of view compared to that of the low aperture objectives used for the two-beam geometry. (iii) Large aperture means high resolution, which is profitable, but in the same time, tight focusing and very high power density (up to about 10^8 W/cm^2). Such intensities often cause heating and optical damage to the sample. Large field of view as well as longer-working distance as provided by the two-beam trap are required in some applications when the objects of interest are of sizes in the 100 μm range, see, e.g., Refs. 6 and 7. An additional disadvantage of the single-beam geometry is the limitation in the vertical stability of the trap, particularly when trapping particles of high refractive index.[13]

The two-beam geometry represents an opposite trade-off. Beams are weakly focused by low aperture objectives, allowing for long WDs, low magnification and large field of view, and moderate intensities ($\leqslant 10^5$ W/cm^2). Drawbacks

are (i) a definitely higher complexity of the optical setup, which needs shaping, aligning, and precisely positioning a couple of counterpropagating beams; and (ii) the trapping geometry depends on the particle size, which in practice means that the beams, interfocal distance Δ must be readjusted if the experiment involves manipulating particles of very different diameters.

In ordinary two-beam arrangements, both beams are generated through a beam splitter and have identical characteristics. They are recombined inside a kind of Sagnac interferometer and are focused by identical objectives,[5,14] in face-to-face configuration. Such setups are built from separate parts, and, apart from the primary function of optically trapping particles, do not offer the image quality and numerous observation tools of commercial microscopes. The goal of the present article is to describe a complete setup, which combines both single- and two-beam trapping. Both functions are integrated into a commercial microscope (Zeiss Axiovert 200M), and are compatible with all observation modes of the microscope. As far as we know, the combination of both short- and long-WD trappings into a single microscope was not achieved before. Below we provide a detailed description of our setup and a sheet of performance data. The article is structured as follows.

(a) Section II is dedicated to the experimental setup. The section starts with an introductory paragraph, which briefly recalls the principles of both kinds of trapping, and exposes the technical problems to be solved for integrating both functions into the microscope. We afterwards describe the optical arrangement around and inside the microscope, and the materials used as tests for optical trapping.

(b) Performance tests of the setup are reported in Sec. III. The goal is to evaluate the performance of optical trapping in both modes on different particles, some of them fluorescent. In the part on single-beam trapping, we essentially characterize the transverse trap efficiency ($Q_\perp$), i.e., the force that holds the particle perpendicularly to the beam axis, for various particles sizes and positions relative to the sample chamber walls. The test procedures are similar to those used in recent works about RP forces and the influence of spherical aberration in optical tweezers.[10,11,15] Long-WD three-dimensional trapping in two-beam mode is demonstrated, and transverse trapping efficiencies are measured as a function of the interfoci distance (Δ), for various particle sizes. In both modes, we test the linearity of the measured trapping force versus the laser power.

(c) The above results are analyzed in Sec. IV. Those for single-beam trapping are compared to results previously reported in the literature. We afterwards discuss the results on two-beam trapping, with emphasis set on the critical issue of axial stability.

(d) The article is summarized and concluded in Sec. V.

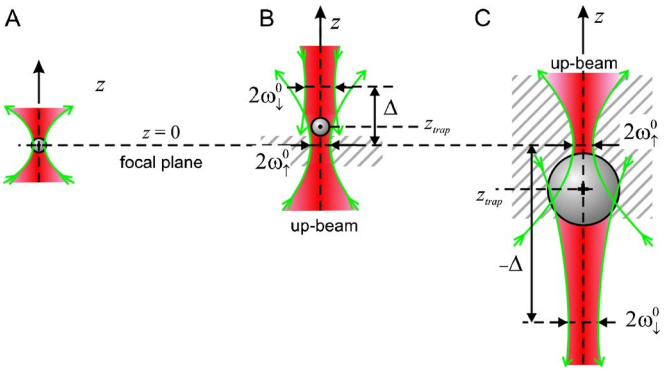

FIG. 1. (Color online) Single (A) and two-beam trappings [(B) and (C)]. Note the change in the sign of Δ, according to whether the particle is small (B) or large (C) compared to the beam waists. The z position of the beads is set by the power ratio of the down- to up beams, $P_\downarrow/P_\uparrow$. The hatched area indicates the altitude limits within which the particle must be trapped to be approximately in focus in the microscope image.

II. MATERIALS AND METHODS

A. Basics

Figure 1 illustrates the basic principles of single-beam [Fig. 1(a)] and two-beam [Figs. 1(b) and 1(c)] traps. As optical tweezers have been the matter of a considerable literature, we do not dwell on the physical principles of single-beam trapping, and rather refer the reader to articles quoted in the reference list,[9,11,12,15,16] and to other references therein. We simply remind that the focal zone of a very large aperture laser beam acts as a three-dimensional (3D) potential well for particles whose index of refraction is larger than that of the surrounding medium. The configuration is built by passing a large waist laser beam through the exit pupil of a large aperture microscope objective, commonly a 100×, numerical aperture (NA) 1.3–1.4 optics.

In the two-beam configuration [Fig. 1(b)], in contrast to single-beam tweezers, the beams are weakly focused. Thus, the wave-front curvature is small and a trapped particle feels each beam as approximately cylindrical. If the beam diameter is much larger than the bead size, refraction and momentum transfer are very efficient within the particle cross section, but a great part of the beam power is lost outside of the particle. In the opposite limit, when the beam waist is much smaller than the bead size, there is no power loss, but there is almost no refraction, and therefore almost no momentum transfer. The optimum in momentum transfer is reached when the beam waist is approximately equal to the particle size. In this situation, the axial component of the radiation pressure force, $F_\parallel(z)$, is maximum. This conclusion is confirmed by calculations, either based on the ray-optics approximation,[17,18] or on the generalized Lorenz-Mie theory (GLMT).[19] We will therefore suppose that $F_\parallel(z)$ only depends on the $a/\omega(z)$ ratio, where a is the particle radius, and $\omega(z)$ the beam radius at altitude z,

$$F_\parallel(z) = q\frac{P}{c}f[\omega(z)/a]. \tag{1}$$

Here the force is supposed proportional to the beam power, P, which is correct in the absence of heating or nonlinear

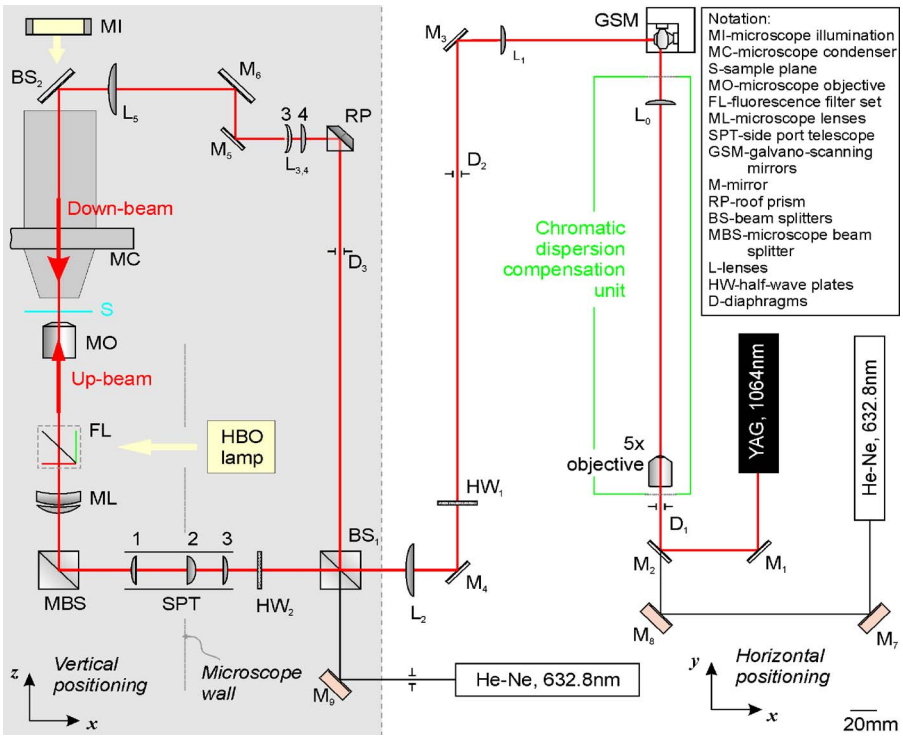

FIG. 2. (Color online) Optical setup. The components on the gray background are mounted on a vertical table, attached to the microscope (the sidewall of the microscope body is indicated with a dashed line). The rest of the setup is horizontally mounted. M_1–M_6 are IR (1064 nm) mirrors. The set of lenses with their respective focal lengths, f, includes L_0 (f=60 mm), L_1 (f=120 mm), L_2 (f=400 mm), $L_{3,4}$ (f_3=35 mm, f_4=50 mm), L_5 (f=150 mm), and SPT (f_1=60 mm, f_2=30 mm, f_3=80 mm). The beam path is drawn to scale in reference to the scale bar (low right corner). All abbreviations are defined in the legend.

effects. q is a prefactor (<1) whose value depends on the particle refractive index. The f function has a maximum for $a/\omega \cong 1$, meaning that the axial force is maximum when the particle is located at a position z such that $a \cong \omega(z)$.

This reasoning allows understanding the way in which a particle can be levitated by a single (weakly focused) vertical beam,[1] and equilibrated against gravity.[20] However, optical levitation does not provide optical trapping, because the particle position strongly depends on the beam power. Trapping can be simply achieved using not one, but a couple of counterpropagating beams. The concept, which has been explored in the 1970s,[2–4,17] and later used in a few applications,[5–8] is illustrated in Figs. 1(b) and 1(c). The middle sketch [Fig. 1(b)] represents the case of a particle which is smaller than both beam waists, denoted $\omega^0_{\uparrow,\downarrow}$. The focus of the down directed ($\downarrow$) beam is located at a distance Δ above that of the up ($\uparrow$) beam. Consider the equilibrium of a particle located between both foci. For simplicity, we may forget about the particle weight, which we may afterwards reintroduce as a perturbation. The particle is pushed by two opposite forces, $F^{\uparrow}_{\parallel}(z)$ and $F^{\downarrow}_{\parallel}(z)$, coming from the up- and down-directed beams, respectively. In the configuration of interest, we have $a/\omega_{\uparrow}(z)<1$ and $a/\omega_{\downarrow}(z)<1$. Note that if a perturbation slightly pushes the particle downwards, then $a/\omega_{\uparrow}(z)$ increases and gets closer to 1, while $a/\omega_{\downarrow}(z)$ decreases. The consequence is that $F^{\uparrow}_{\parallel}(z)$ increases and $F^{\downarrow}_{\parallel}(z)$ decreases, resulting in a positive restoring force. The same conclusion of course holds in the opposite situation where the particle is slightly pushed upwards. The configuration provides stable three-dimensional trapping. Figure 1(c) shows the alternate situation of a particle bigger than both beam waists. In this case, stable trapping implies locating the down beam waist below the up beam waist, a condition which we denote as $\Delta<0$ [conversely $\Delta>0$ in Fig. 1(b)].

Note that in both types of equilibrium, the final z position of the trapped particle depends on the power repartition between both beams. In the experiments described below, we use this property to bring the particle in focus in the microscope image.

In Sec. II B we describe the implementation of Figs. 1(a)–1(c) geometries in a Zeiss Axiovert 200M inverted microscope. The up and down beams are generated from a single primary laser beam, as in anterior designs. The up beam is passed through a side video port at the lower part of the microscope body, while the down beam, only used in long-WD trapping, is passed through the microscope condenser, above the objective (a 40× in this case). Both beams go through intermediate optics, described below, whose purpose is to arrive at focused beams of similar characteristics inside the sample. The optical trap, in both modes, can be scanned in the horizontal plane, by means of a couple of motorized mirrors acting on the primary beam.

B. Optical setup

Microscope. The heart of the setup (Fig. 2) is a computerized and motorized inverted light microscope Axiovert 200M of Zeiss (Jena, Germany) allowing observation in phase contrast, differential interference contrast, bright field, and fluorescence microscopy. A 100×, Ph3, NA=1.4 oil immersion objective (Plan Apochromat 100×), and a 40×, Ph2, NA=0.6, W.D.=1.8 mm objective (LD Achroplan 40×) were used in single- and two-beam modes, respectively. The microscope condenser characteristics are NA=0.55 and WD=26 mm. To allow working in phase contrast mode in the double-beam configuration of the setup, we used a custom-made filter (Präzisionsoptik Gera GmbH, Germany) with a phase ring (Ph2). The filter was transparent for

IR resulting in negligible power losses (<1%) for the down beam. In vertical direction, the microscope focus knob is motorized and computer controlled, allowing displacement of the objective with a 50 nm resolution. The microscope is also equipped with a motorized computer controlled stage (LStep 13, Märzhäuser, Germany) for displacement in the *xy* plane. An additional *z*-positioning stage with a microscrew drive (Narishige, Japan) attached to the motorized *xy* stage is used to displace the sample chamber in *z* direction when two-beam trapping configuration is used. In this way the condenser, the objective, and the sample can be displaced vertically independently from each other. Images of trapped particles, in incoherent light (transmission or fluorescence), are captured by a digital camera (Cool Snap HQ, Roper Scientific, US) through the front camera port of the microscope. The camera is controlled by a computer, which is used for image analysis performed with Simple PCI software. The second camera port is equipped with an IR camera (LaserCam IIID beam profiler, Coherent, US), for beam analysis and tuning purposes. The IR detector is used to measure the waists of the two beams in the double-beam mode.

Primary beam. A schematic drawing of the system is presented in Fig. 2. The system is fed by a continuous wave Nd:YAG (yttrium aluminum garnet) laser (Spectra Physics, US), wavelength 1064 nm, TEM_{00} mode, and maximum output power of 5 W. The position of the optical trap inside the microscope observation plane is driven by a couple of computer controlled galvano-scanning mirrors (GSI Lumonics GmbH, Germany; the tick frequency of the scan controller is 43.4 KHz), denoted as GSM in Fig. 2. The pair of lenses L_1 and L_2 constitutes a telescope, which forms an image of the GSMs in the back focal plane of the microscope objective (MO). This telescope expands the beam so that it completely covers the pupil of the objective. We noticed the presence of an important chromatic dispersion, between 1064 nm and the visible spectrum, with both objectives used for trapping: the 100× objective focuses the IR beam about 2 μm above the observation plane; the shift is 50 μm with the 40× objective. The purpose of the "chromatic dispersion compensation unit," indicated in the figure, is to bring the IR beam waist back in the observation plane. The unit is made of a 5× objective plus a plano-convex lens L_0, whose separation can be adjusted to achieve the compensation. The unit was used only for correcting the aberrations of the 40× objective. Thus, switching between the two modes of operation, single- and double-beam trappings, essentially requires installing or removing the chromatic dispersion unit and exchange of the objectives.

All optics dedicated to directing and shaping the primary beam are installed on a horizontal table, together with the microscope. A He–Ne laser and an infrared viewer (Photon View, Coherent) are used for alignment. The polarizing beam-splitter cube BS_1 splits the primary beam into a couple of secondary beams, the "up" (clockwise) and "down" (counterclockwise) beams, respectively. The power repartition between both beams is tuned by rotating the half-wave plate HW_1 located before BS_1.

The *up beam* is used both in single- and double-beam trapping modes. Single-beam trapping demands a collimated beam to be passed through the MO rear focal plane. In most microscope designs, this plane is directly visible by reflection through a video port. This is so, for instance, with the Zeiss Axiovert 135 microscope. In this "classical" situation, it suffices to pass the beam through the port to feed the optical trap correctly. The configuration of the primary beam, in our setup, is "classical," meaning that one could, for instance, use it to feed an optical trap in an Axiovert 135 microscope. A complication arises in the case of the Axiovert 200M microscope (making the instrument "nonclassical") because of the presence of an intermediate imaging optics (a microscope tube lens, denoted as ML in Fig. 2) between the objective and the beam splitter. The laser beam of course does not remain collimated through this optics, and the image of the GSMs is no longer formed inside the MO pupil. We solved this problem by means of a three-lens unit (denoted as SPT in Fig. 2), which was fitted to the microscope body through the side video port. The purpose of the SPT is twofold: (i) the ML+SPT set acts as a telescope, of −1 magnification; and (ii) from outside of the microscope, the image of the MO pupil through the microscope optics+SPT coincides with itself. The SPT thus virtually eliminates the presence of the ML, and emulates the above-mentioned "classical" configuration.

The *down beam* is guided and configured through a few optics installed on a small vertical table, attached to the microscope body. A second red laser is used for alignment of the down beam specifically. The microscope condenser (MC) now serves as an objective, similarly to MO. The IR beam is reflected by BS_2, which is transparent for visible light (and thus not hindering the microscope illumination). The $L_{3,4}+L_5$ set of lenses acts as a telescope to expand the beam up to about the size of the MC pupil, i.e., the microscope aperture diaphragm, and conjugates the GSMs onto the MC pupil plane.

Scanning. A particle trapped in the sample solution can be moved in two ways: by keeping the beam at a fixed location and displacing the microscope stage, or by keeping the stage fixed and displacing the beam (scanning). Note that with particle movement we imply displacing the bead with respect to the solution media and not necessarily with respect to the laboratory coordinates. The chamber displacement is computer controlled via the motorized stage, with a velocity in the 0.001–40 mm/s range in the *x*-*y* plane. Scanning is performed by means of the GSMs, whose motion can be computer driven for guiding the beam along a programed trajectory, or for splitting the beam into multiple traps.[21]

Operating the scanning mode with the single-beam trap is straightforward. In the double-beam mode, care must be taken so that the up and down beams, in the sample plane, are moved in the same directions ($\Delta x^{\uparrow} \| \Delta x^{\downarrow}$ and $\Delta y^{\uparrow} \| \Delta y^{\downarrow}$) and with the same magnification ($\Delta x^{\uparrow} = \Delta x^{\downarrow}$ and $\Delta y^{\uparrow} = \Delta y^{\downarrow}$). Direction matching depends on the many reflections along both beam paths. This is the reason why we had to install a roof prism (RP) instead of a simple mirror on the down-beam path. Compared to a simple plane mirror, this prism changes the sign of $\Delta x^{\downarrow}$, with no change in amplitude. Amplitude matching is obtained through an appropriate choice of the focal lengths of $L_{3,4}$ and L_5 objectives. The reasoning

TABLE I. Characteristics of the particles used in this work.

Particle diameter, $2a$ (μm)	Composition, surface groups	Refractive index	Density, (g/cm^3)	Other specifications	Producer
0.984±0.023	Polystyrene (latex)	1.59 (vis) 1.57 (IR)[a]		—	Polysciences, Inc., Warrington, PA
2.06±0.024					
6.359±0.451					
10.143±0.638					
16±2.56					
5.804±0.511	Latex Fluoresbrite™ carboxy BB		1.05	Colored,[b] λ_{ex}=360 nm λ_{em}=407 nm	
2.82±0.135	Latex, Fluoresbrite™ plain YG			Colored,[b] λ_{ex}=455 nm λ_{em}=515 nm	
4±0.2	Latex, Fluospheres® sulphate microspheres			Fluorescent,[b] λ_{ex}=580 nm λ_{em}=605 nm	Molecular probes, Eugene, Oregon

[a]See Ref. 11 for details.
[b]The excitation and emission wavelengths are denoted as λ_{ex} and λ_{em}, respectively.

is as follows: the $(L_{3,4}+L_5)$ set is a telescope, whose magnification should match that of the (MO+condenser) set, i.e., the corresponding focal length ratio, f_{MC}/f_{MO}. This is the first condition. The second condition is that the image of the GSMs, along the down path, has to be located in the plane of the condenser aperture diaphragm. This imposes the value of $f_{L_5}+f_{L_{3,4}}$, about 175 mm in our setup. The above conditions result in $f_{L_5}\cong 150$ mm and $f_{L_{3,4}}\cong 24$ mm. In the setup, $f_{L_5}=150$ mm. $L_{3,4}$ is a two-lens set. The position of this set, and the separation between both lenses inside were experimentally tuned to meet the ($\Delta x^{\uparrow}=\Delta x^{\downarrow}$ and $\Delta y^{\uparrow}=\Delta y^{\downarrow}$) condition. Amplitude matching was verified directly from the traces of both beams inside the sample plane, by means of the beam profiler camera. An indirect verification was performed by means of a trapped particle, in two-beam mode. The particle could be scanned across a ±20 μm excursion in x while 3D trapping was maintained.

With this configuration, we estimated the beam waists of both beams in the sample plane from their far-field diffraction patterns: $\omega_0^{\uparrow}\cong 1.5$ μm and $\omega_0^{\downarrow}\cong 2.5$ μm, for the up and down beams, respectively. Note that the configuration is not symmetrical, but this is not a problem since up-down symmetry ($\omega_0^{\uparrow}=\omega_0^{\downarrow}$) is not required for the two-beam trap geometry to work.

Power losses. All optical components, except those located inside the microscope, have coatings optimized for 1064 nm. The loss in beam power from the Nd:YAG laser head to the objective pupil is 81%. Both of the used objectives additionally reduce the power. The power loss in the IR range for the 40× objective is 71% according to information by producer (Zeiss, Germany). For the 100× objective we did not have the corresponding information, except for a similar objective but without the phase ring inside (the reported power loss in the IR range for that objective is ~75%). We estimated the losses in the following way (see also Refs. 22 and 23): we used a second objective, identical to the 100× one. The two objectives were assembled in a face-to-face configuration and aligned on the beam path. An immersion oil droplet was placed in between and the two focal planes were brought together. The output power transmission measured after the pupil of the second objective was 2.1%, which gives 85.5% for the power loss for each objective. This value is somewhat low compared to values given in Ref. 23, but the latter were measured for objectives without phase rings. The power losses due to the sample chamber and solution were not estimated and the data given in this work do not account for them. The loss for the down beam, from BS_1 to the sample plane, is 44%. Thus, starting from the 5 W source, the maximum power in the sample plane is about 140 mW in single-beam trap, and about 270 mW in double-beam trap mode.

C. Materials

Polystyrene (latex) particles of different sizes were used in this work. Their properties are summarized in Table I. The working solutions were prepared by dilution of the latex suspensions as obtained from the producer (2.65% solids-latex) with pure Millipore water. For operation with the single-beam tweezers, the sample solution was placed in a chamber consisting of a glass slide of thickness of 0.17 mm, an objective glass, and a Parafilm spacer (50–70 μm in thickness). For the double-beam trap experiments, we simply used a closed quartz cuvette (Hellma, Germany) of wall thickness=1.25 mm and working path=1 mm.

Except for the 0.984 and 2.06 μm particles, which were close to monodisperse (±0.024 μm), the suspensions were definitely polydisperse and it was necessary to determine the particle radii (a) individually. We used two different procedures:[6] (i) image analysis: this method was restricted to large particles, $a\geqslant 5$ μm, and the accuracy was ±0.15 μm. (ii) Sedimentation: measuring the sedimentation velocity, v_{sed}, of a particle in bulk water yields the hydrodynamic radius, $a_H=\sqrt{9\eta v_{sed}/2g\Delta\rho}$, where η is the water viscosity, g

the gravity acceleration, and $\Delta\rho$ the density difference between water and the particle material. The sedimentation velocity was obtained by measuring the times at which a particle crosses several z levels in the chamber; a linear fit through the z versus time data gives the sedimentation velocity with high accuracy. The error in the particle size determination was 1% for particles larger than 5 μm and about 5% for the smaller particles.

III. RESULTS

This section describes several experiments illustrating the trapping efficiency of the setup, in both configurations. As in prior works,[10,11,24] the transverse trap efficiency was estimated from the maximum transverse trapping force. The procedure consists in moving the sample stage horizontally at constant velocity v, up to a critical value $v=v_{\mathrm{esc}}$, beyond which the particle escapes out of the trap. The corresponding force is given by

$$F_{\perp} = 6\pi\eta a v_{\mathrm{esc}}. \tag{2}$$

In the simplest form, the left-hand side of the above equation is the Stokes drag of the particle inside an unbounded fluid (water in our experiments) of shear viscosity η. This is approximately so in the two-beam (LWD) trap experiments, because the particle is about in the middle of the sample chamber, far from the walls. In the single-beam trapping experiments, the particle is very close to the bottom wall of the chamber, because of the short-working distance of the microscope objective. Hydrodynamic coupling to the wall definitely increases the drag. Equation (2) still holds, but with an effective viscosity $\eta_{\mathrm{eff}} > \eta$. Applying the bare Eq. (2) in this circumstance only provides an apparent trap force, $F_{\perp}^{(0)}$, which is less than the true force, $F_{\perp}=kF_{\perp}^{(0)}$. The hydrodynamic coupling factor $k=\eta_{\mathrm{eff}}/\eta$ only depends on the a/h ratio, where h is the distance between particle center and the wall.[25]

The trap efficiency gives an estimate of the restoring force that brings the particle back to the beam axis when it is slightly pushed outwards. Strictly speaking, the restoring force is best characterized by the trap stiffness: $k_{\perp}=dF_{\perp}/dr$ (r is the distance of the particle center to the beam axis), in the $r\to 0$ limit (accurate methods to measure trap stiffness are described in the literature, see, e.g., Refs. 26 and 27). In general, $F_{\perp}$ is larger than $k_{\perp}a$, but on the same order of magnitude; therefore $F_{\perp}/a$ provides an estimate of the trap stiffness, which is enough to compare the performances of different setups.

In two-beam trap mode, axial stability was only studied qualitatively, by switching on and off one or both laser beams. The single-beam trap was found axially stable near the observation plane for all small particles up to 4 μm. We could not stably trap particles $\geqslant 5$ μm in diameter in the single-beam mode. Not surprisingly, axial stability in the double-beam mode was found to depend on a and Δ, as we explain below.

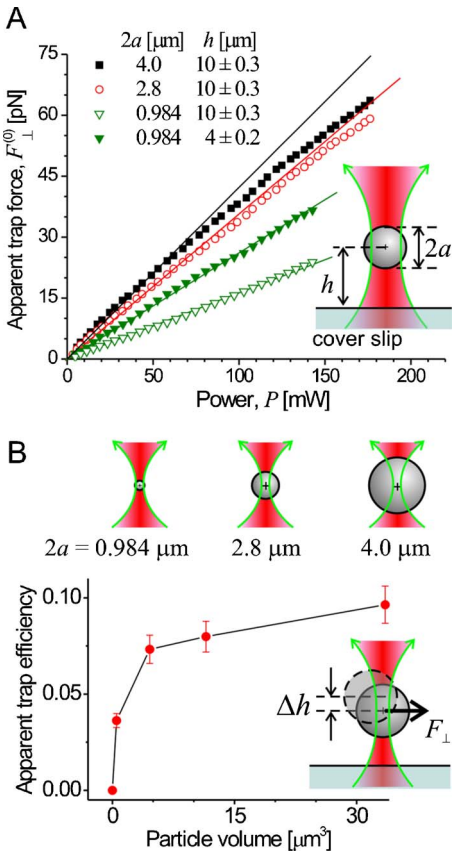

FIG. 3. (Color online) (A) Transverse RP force [as defined in Eq. (2)] exerted by the single-beam trap, as a function of the laser beam power, for different sizes of polystyrene spheres in water. The apparent trap force, $F_{\perp}^{(0)}$, was measured at different distances, h, above the cover slip. (B) The apparent trapping efficiency $Q_{\perp}^{(0)}$ obtained from the slopes of the linear fits in (A) for $h=10\pm0.3$ μm, vs particle volume. The inset below the graph illustrates the shift in h induced by the horizontal motion of the sample stage. Note (see the sketch on top) that the beam intercepts about the full volume of the smallest particles ($2a\approx 1$ μm), but only a fraction of the volume of the largest ones ($2a\approx 4$ μm).

A. Single-beam trap

Latex particles of various sizes were trapped and the escape velocity was measured at different distances, h, above the chamber bottom boundary; see the inset of Fig. 3(a) for the definition of h. In this paragraph, we only provide bare data, in the form of the above defined "apparent trap force." The hydrodynamic correction will be shortly discussed in Sec. IV A. The results are shown in Fig. 3(a) as a function of the beam power, P.

In principle, RP forces (these include gradient and scattering forces) should simply be proportional to P. The data show that the proportionality of $F_{\perp}^{(0)}$ to P is verified for moderate powers whatever the particle size. However, definite deviations are evidenced for 2.8 and 4 μm particles, above powers of 90 and 70 mW, respectively. For these two particle sizes, the apparent trap efficiency decreases with power.

The apparent transverse trap efficiency, $Q_{\perp}^{(0)}$, is defined in the linear domain through the relation $F_{\perp}^{(0)}=nQ_{\perp}^{(0)}P/c$. Here, n is the refractive index of the immersion phase, water in our experiments ($n\cong 1.34$); and c is the velocity of light. The graph in Fig. 3(b) shows the variation of $Q_{\perp}^{(0)}$ as a function of the particle volume, $V=(4/3)\pi a^3$. In the small par-

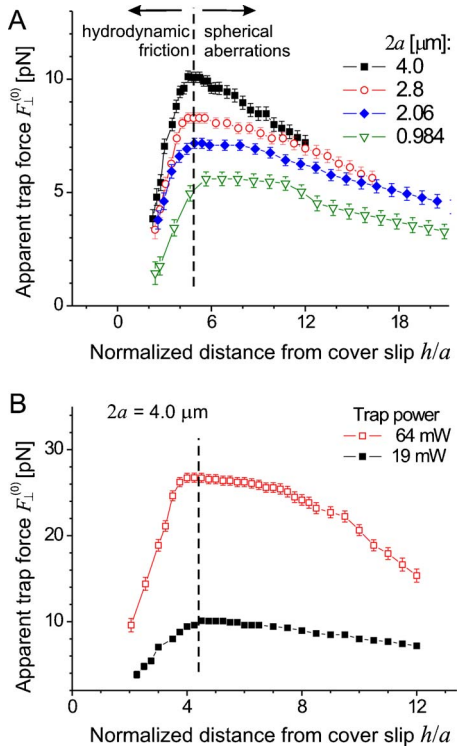

FIG. 4. (Color online) Apparent transverse trap force $F_\perp^{(0)}$ as a function of the rescaled distance to wall, in (A) for different particle sizes, at constant beam power=19 mW; in (B) for two different powers with the same particle. The crossover distance is approximately two particle diameters as shown with the dashed line.

ticle size limit (the Rayleigh regime, $a \ll \lambda$), we expect that the trap efficiency scales as $Q_\perp \propto V$.[9,18] In our experiments, the particles are not in this regime, being comparable to or definitely larger than the wavelength. As can be seen from the graph, the apparent trap efficiency increases with V, but the increase is much weaker than that in the Rayleigh limit. Error bars in the $(Q_\perp^{(0)}, V)$ graph are estimated from the statistical scatter of measured escape velocities. The inset at the bottom of Fig. 3(b) illustrates another source of error, coming from the fact that the particle in general does not escape out of the trap in a horizontal plane. The flow slightly lifts the particle above the focus plane. The effect is hardly detectable with small particles, but is very clear with bigger ones. Thus, the measured trap efficiency is not strictly a transverse one, being contributed in part by an axial component.

As demonstrated in Fig. 3(a), $Q_\perp^{(0)}$ also depends on the height above the cover slip, h (compare the two data sets for the 0.984 μm particles). Figure 4(a) shows the results of experiments carried out at constant P as a function of h for different particle sizes. Notice that $F_\perp^{(0)}(h)$ goes through a maximum in h in each case, on the order of two particle diameters. This trend remains the same whatever the beam power, as shown for the 4 μm particles in Fig. 4(b). The fact that $F_\perp^{(0)}$ increases at small h and decreases at large h is in line with previously reported data, and can be simply interpreted, as we explain in the discussion.

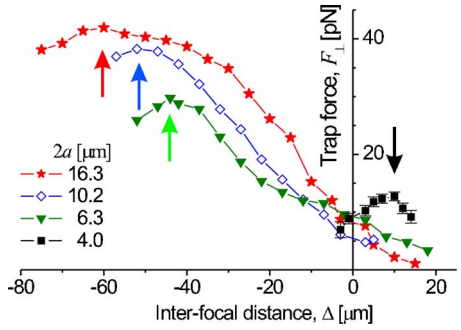

FIG. 5. (Color online) Double-beam lateral trap force, $F_\perp$, as a function of the interfocal distance for polystyrene spheres of different sizes in water. The error in Δ is ± 4 μm and the error in the measured force is approximately represented by the size of the symbols used. Δ_{max} is indicated for each particle size by an arrow with the color of the corresponding data set. All measurements were performed at total beam power of 114 mW.

B. Double-beam long-working-distance optical trap

As explained in Sec. II A, the stability of the double beam depends on the interfocal distance Δ. Figure 1(b) shows the case of a positive Δ, i.e., when the beam waist of the down beam $(\omega_0^\downarrow)$ is located above that of the up-going beam $(\omega_0^\uparrow)$. Conversely, in Fig. 1(c), Δ is negative, meaning that $\omega_0^\downarrow$ is below $\omega_0^\uparrow$. Adjusting the setup to these two configurations is simply performed by moving the microscope objective in vertical direction, z, with respect to the condenser position. For given particle characteristics, the configuration is tested for axial stability by alternately switching on and off the up and down beams.

In principle, stable trapping of small particles [Fig. 1(b)] is achieved with $\Delta > 0$ configurations, while big particles demand $\Delta < 0$ configurations [Fig. 1(c)]. The sketches in Figs. 1(b) and 1(c) represent realistic configurations, with $2a = 4$ μm, $\Delta = -10$ μm in (B), and $2a = 10$ μm, $\Delta = 30$ μm in (C). The beam waists ($\omega_0^\uparrow = 1.5$ μm and $\omega_0^\downarrow = 2.5$ μm) and diffraction lengths are in scale with the particle size and interfocal distance.

For a given configuration and beam powers $(P_\downarrow, P_\uparrow)$, the particle is trapped between both beam waists, at an altitude denoted as z_{trap} in Figs. 1(b) and 1(c). When the RP forces are much larger than the particle weight, for given particle characteristics, z_{trap} mainly depends on the $P_\downarrow / P_\uparrow$ ratio, whose value is controlled by rotating the HW_1 half-wave plate (Fig. 2). The position of the plate is tuned in such a way that z_{trap} is located close to the up-beam waist, which is also the microscope observation plane ($z=0$). This is a necessary condition; otherwise, observation is not possible as the particle is out of focus. The tolerance, corresponding to the hatched zones in Figs. 1(b) and 1(c), is about a couple of particle diameters, i.e., $|z_{trap}| < 2a$, where observation is still possible.

Figure 5 shows data about the two-beam trap stability for different configurations, i.e., when Δ is varied, and for different particle sizes. The total beam power is kept constant, $P = P_\uparrow + P_\downarrow = 114$ mW, while $P_\downarrow / P_\uparrow$ is tuned to meet the $|z_{trap}| < 2a$ condition. All experimental points correspond to three dimensionally stable trapping. We measured the transverse trap efficiency in each case, using the same procedure as for the single-beam trap. The long-working distance of the

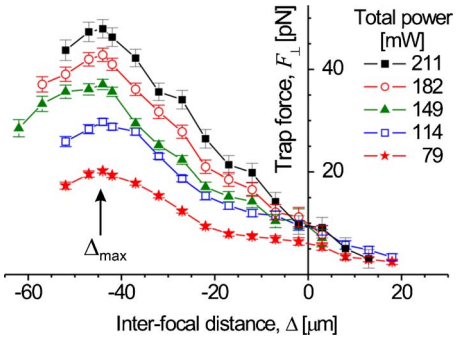

FIG. 6. (Color online) Lateral trap force $F_\perp$ exerted by the tweezers in double-beam trap configuration as a function of the interfocal distance for different total beam power. The measurements were performed with a sphere of diameter $2a=6.3$ μm. The error in Δ is ± 4 μm. The position of maximum trapping force ($\Delta_{max} \cong -45$ μm) is indicated with an arrow.

two-beam trap allowed us to hold the trapped particle far from the cell boundaries ($h \geqslant 50$ μm), well away from wall effects. The data show that $2a=4$ μm particles behave as "small" particles, according to the above defined classification, i.e., are only trapped in a $\Delta > 0$ configuration, while those with $2a \geqslant 6$ μm behave as "big" ones, imposing $\Delta < 0$. For each particle size, we find that $F_\perp$ goes through a maximum for a particular interfocal distance, Δ_{max}, indicated by an arrow in the graph. The Δ_{max} configuration thus provides the optimal transverse stability. Note that the value of Δ_{max} definitely depends on the particle size.

The effect of changing the total beam power is illustrated with a single particle size ($2a=6.3$ μm) in Fig. 6. The same procedure as before was repeated, searching for the maximum transverse trapping force. The data indicate that $F_\perp(\Delta)$ scales proportionally to P, meaning that the particle weight is about negligible in the explored range of powers and that RP forces are simply proportional to the total beam power. A direct consequence is that Δ_{max} is about independent of P.

We further investigated the linearity of RP forces by measuring $F_\perp^{max}=F_\perp(\Delta_{max})$ for different particle sizes as a function of P. The results, displayed in Fig. 7, clearly show that the force remains proportional to P, in the full power range, for all sizes and whatever the particles are fluorescent or not. Note that the forces achieved for $2a=4$ μm particles are comparable with those applied by single-beam tweezers

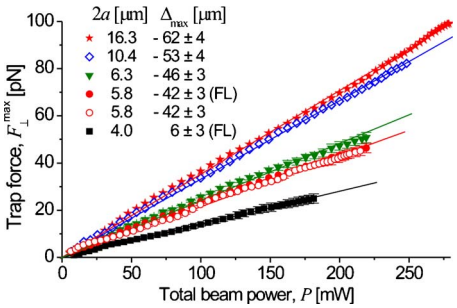

FIG. 7. (Color online) Maximum transverse trapping force in double-beam configuration as a function of the incident laser power, for different polystyrene spheres in water. The error in the force measurements with the largest beads is approximately equal to the symbol size. The two smallest particles have been manipulated both in fluorescent mode (indicated with "FL" in the legend) and in bright field.

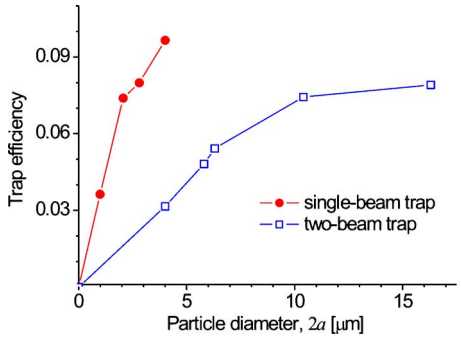

FIG. 8. (Color online) Transverse trap efficiencies, in single- and double-beam configurations, as a function of latex particle diameter.

at the distance of ~2 particle diameters away from the chamber wall (recall that this is the distance where the apparent transverse trap force $F_\perp^{(0)}$ is highest); see Figs. 3(a) and 4(a).

A question arises about fluorescent particles concerning a possible influence of the microscope observation mode on the optical trapping equilibrium.[13] For most of the tests, the microscope was operated in simple transmission (bright field). The fluorescence mode implies adding a dichroic beam splitter, denoted as FL in Fig. 2, below MO, to direct the excitation light towards the sample through MO. This additional element on the up-beam path and the slight heating of the particle due to fluorescence excitation may perturb the optical trapping. The performance of the optical trap was tested in both microscope modes with $2a=5.8$ μm fluorescent particles. The results (Fig. 7, open and filled circles for transmission and fluorescence mode, respectively) indicate that operating the microscope in fluorescence mode does not modify the trapping of the fluorescent particles, within experimental error, whatever the YAG laser beam power.

IV. DISCUSSION

We gathered in Fig. 8 the measurements of transverse trap efficiencies in both single- and double-beam configurations. Those for the single-beam mode are apparent efficiencies, as defined in Sec. III. Note that the measured values of $Q_\perp$, in two-beam mode, are lower (though of same order) than those of $Q_\perp^{(0)}$ in single-beam tweezers. The difference between the efficiencies of both modes is not surprising, since transverse RP forces are highest when the beam diameter is small compared to the particle size.[4,19] Below, we analyze the experimental data corresponding to single- and double-beam modes. In principle, a complete quantitative discussion of the experimental data is possible, using the generalized Lorenz-Mie theory[19] or other representations.[28] However, taking into account all the experimental variables in all geometries ($\omega_\uparrow^0, \omega_\downarrow^0, P_\uparrow, P_\downarrow, \Delta, a, n,$) makes the simulation complex, a task that should be the matter of a dedicated analysis. In the spirit of this article, we restrict the following discussion to qualitative points.

A. Single-beam trap

In the single-beam mode, measurements are complicated by the proximity of the cell wall, which causes both hydrodynamic and optical problems.

The increase in $F_{\perp}^{(0)}$ in the $0 \leqslant h/a \leqslant 5$ interval (Fig. 4) is only apparent, being caused by the hydrodynamic coupling of the particle with the wall. In theory, this artifact can be eliminated by applying a correction factor to the measured escape force,[10,11,25]

$$k = \left[1 - \frac{9}{16}(a/h) + \frac{1}{8}(a/h)^3 - \frac{45}{256}(a/h)^4 - \frac{1}{16}(a/h)^5\right]^{-1}. \tag{3}$$

The correction is very sensitive to the value of h in the $h/a \to 1$ limit, which means that measuring $F_{\perp}$ with a particle very close to the cell wall requires a very accurate measurement of the gap between the particle and the wall. Note that the measurement should take into account the chromatic aberration of the 100× objective (as mentioned in Sec. II B). Because of these difficulties, we did not attempt to correct our data using Eq. (3). Fortunately, the maximum of $F_{\perp}^{(0)}$ occurs for $h/a \approx 4$, corresponding to $k \approx 1.16$, i.e., the corresponding hydrodynamic effect is weak. In other words, the maximum of $F_{\perp}^{(0)}$, in Fig. 4, and data to the right of the maximum need about no correction: $F_{\perp}^{(0)} \cong F_{\perp}$ and $Q_{\perp}^{(0)} \cong Q_{\perp}$ for $h/a > 4$. Therefore the single-beam trap efficiencies displayed in Fig. 8 have been simply estimated from the maximum of each $F_{\perp}^{(0)}$ vs h/a graph.

The optical problem related to the distance from the cell wall is spherical aberration.[10,11,15,24,29,30] Conversely to the hydrodynamic coupling, the spherical aberration increases when h/a increases, causing the decrease of $F_{\perp}$ for $h/a > 5$ (see Fig. 4; note that in this region $F_{\perp}^{(0)} \cong F_{\perp}$). The decreasing branches of the $F_{\perp}(h/a)$ curves (Fig. 4) can be extrapolated down to the $h/a \to 0$ limit, in an attempt to eliminate the effect of spherical aberration. This tentative correction, giving the trap efficiency in the limit of no spherical aberration, increases the value of $Q_{\perp}$ by about 40% for the $2a = 4$ μm particles, and by about 30% for the smaller ones ($2a = 1$ μm).

The data for the single-beam trap in Fig. 8 confirm the conclusions of previous works,[10,11] according to which the trap efficiency increases with the particle diameter. Though similar in order of magnitude, our values are lower than those of Wright *et al.*[11] and Felgner *et al.*[10] for $2a = 1$ μm, we find $Q_{\perp} \cong 0.037$, to be compared to 0.08,[10] (this measurement was performed in glycerol solution) and 0.13.[11] Taking into account the above remarks on hydrodynamic coupling and spherical aberration, our value may be raised up to about 0.048, still below the other values. One may infer that we still underestimate the trap efficiency because of the lift effect [denoted as Δh in Fig. 3(b)] which we mentioned in Sec. III A, but this complication probably existed in the other works too. Another possible explanation is related to the fact that our 100× objective is with a Ph3 phase ring which was not the case for the objectives used by Felgner *et al.*[10] and Wright *et al.*[11] In addition, the power losses due to the sample presence were not taken into account (see Sec. III B on power losses).

We noticed deviations of $F_{\perp}$ from linearity versus the beam power, especially with the fluorescent particles [Fig. 3(a)]. This is probably due to a slight heating of the particle and of the fluid around it.[31] Note that permanent optical damage of the trapped particles is ruled out, as no hysteresis in the data was observed when changing the power. However, the reason why this heating causes the nonlinearity in $F_{\perp}(P)$ is not clarified. Water convection[31] around the particle is unlikely, because of the close proximity of the cell wall.[32] Thermal lensing is a possible mechanism, which might decrease the amount of momentum transfer between light and the particle.

B. Double-beam trap

In contrast to the measurements with a single-beam trap, the transverse trap force is strictly linear with power in the double-beam mode [compare Fig. 7 with Fig. 3(a)]. This is not surprising, because both beams are moderately focused and cannot produce large temperature gradients as in the focal region of the high aperture objective. Note that the two-beam trapping mode is potentially much more sensitive to thermally induced water convection,[31] because the particle is far from the cell walls. If the laser light is partly absorbed, the particle and the fluid close to it play the role of a hot spot, and are the source of a convection flow inside the cell. However, and fortunately enough, this potential complication was not detected in our experiments.

The configurations used for the experiments reported in Sec. III B were arrived at empirically, with just the twofold requirement of axial stability and observability ($|z_{\mathrm{trap}}| < 2a$). A configuration of the two-beam trap is specified by the value of Δ and those of the beam powers, $P_{\uparrow,\downarrow}$. The data displayed in Fig. 5 are sets of three dimensionally stable configurations, for which we measured the corresponding transverse trap efficiencies. Axial stability was only tested qualitatively, as we explained, but this simple testing allows us to verify the rules that we stated based on Eq. (1). Experiments indeed confirm that stable trapping of small particles ($a = 2$ μm) implies $\Delta > 0$, while Δ has to be negative for big particles ($a > 3$ μm). The crossover particle diameter therefore is between 4 and 6 μm. This estimate is about in line with what might be expected from the measured values of the beam waists, $2\omega_{\uparrow}^{0} \cong 3$ μm and $2\omega_{\downarrow}^{0} \cong 5$ μm.

V. CONCLUDING REMARKS

We have built and characterized a setup that provides both short-working (SW) and long-working (LW) distance optical trappings, whose heart is a commercial Zeiss Axiovert 200M microscope. The trapping functions are compatible with the microscope observation tools, in transmission, fluorescence, and phase contrast.

Both trapping modes (SW and LW) follow the classical principles of optical tweezers and two-beam trapping, respectively, but implementing them into the microscope implied solving specific technical problems: shaping the up beam through the tube-lens optics of the Axiovert 200, and guiding and shaping the down beam through the microscope condenser.

We characterized the performance of the setup in both modes. The performance of the optical tweezers mode was found comparable to those of other experiments,[10,11] with

similar findings about the roles of spherical aberration and the hydrodynamic coupling to the sample chamber boundaries. We systematically explored different configurations in the two-beam mode, and experimentally found those providing the best trapping efficiencies. We further verified that the observed equilibrium characteristics could be understood from simple physical principles.

The observations were carried out with spherical particles of different sizes between 1 and 16 μm, some of them fluorescent. We checked that operating the microscope in fluorescence, in the visible domain, was fully compatible with optical trapping by the YAG laser beam(s).

We end this summary with practical information about the level of difficulty to tune and operate the setup. Our experience is that a few hours are sufficient to learn, and about 15 min for a trained user to go through all tuning steps. As a whole, the setup is definitely more complex than the basic optical tweezer arrangement, but remains reasonably easy to operate.

ACKNOWLEDGMENT

Günter Haseloff is acknowledged for machining various adapters and optics holders.

[1] A. Ashkin, Phys. Rev. Lett. **24**, 156 (1970).
[2] G. Roosen, thesis, Université Paris XI, 1978.
[3] G. Roosen and C. Imbert, Phys. Lett. **59A**, 6 (1976).
[4] G. Roosen, Opt. Commun. **21**, 189 (1977).
[5] T. N. Buican, D. L. Neagley, W. C. Morrison, and B. D. Upham, Proc. SPIE **1063**, 190 (1989).
[6] R. Dimova, B. Pouligny, and C. Dietrich, Biophys. J. **79**, 340 (2000).
[7] C. Dietrich, M. I. Angelova, and B. Pouligny, J. Phys. II **7**, 1651 (1997).
[8] P. J. Rodrigo, V. Ricardo Daria, and J. Glückstad, Opt. Lett. **29**, 2270 (2004).
[9] A. Ashkin, J. M. Dziedzic, J. E. Bjorkholm, and S. Chu, Opt. Lett. **11**, 288 (1986).
[10] H. Felgner, O. Muller, and M. Schliwa, Appl. Opt. **34**, 977 (1995).
[11] W. H. Wright, G. J. Sonek and M. W. Berns, Appl. Opt. **33**, 1735 (1994).
[12] D. G. Grier, Nature (London) **424**, 810 (2003).
[13] R. R. Agayan, F. Gittes, R. Kopelman, and C. F. Schmidt, Appl. Opt. **41**, 2318 (2002).
[14] M. I. Angelova and B. Pouligny, J. Opt. A, Pure Appl. Opt. **2**, 261 (1993).
[15] A. Rohrbach and E. K. H. Stelzer, Appl. Opt. **41**, 2494 (2002).
[16] S. M. Block, in *Noninvasive Techniques in Cell Biology* (Wiley-Liss, New York, 1990), p. 375.
[17] G. Roosen, B. Delaunay and C. Imbert, J. Opt. (Paris) **8**, 181 (1977).
[18] T. C. Bakker Schut, G. Hesselink, B. G. de Groot and J. Greve, Cytometry **12**, 479 (1991).
[19] K. F. Ren, G. Gréhan, and G. Gouesbet, Opt. Commun. **108**, 343 (1994).
[20] A. Ashkin and J. M. Dziedzic, Appl. Phys. Lett. **19**, 283 (1971).
[21] H. Misawa, K. Sasaki, M. Koshioka, N. Kitamura, and H. Masuhara, Appl. Phys. Lett. **60**, 310 (1992).
[22] H. Misawa, M. Koshioka, K. Sasaki, N. Kitamura, and H. Masuhara, J. Appl. Phys. **70**, 3829 (1991).
[23] K. C. Neuman, E. H. Chadd, G. F. Liou, K. Bergman, and S. M. Block, Biophys. J. **77**, 2856 (1999).
[24] E. Fällman and O. Axner, Appl. Opt. **42**, 3915 (2003).
[25] J. Happel and H. Brenner, *Low Reynolds Number Hydrodynamics*, 3rd ed. (Martinus Nijhoff, The Hague, 1983).
[26] F. Gittes and C. Schmidt, Opt. Lett. **23**, 7 (1998).
[27] K. Berg-Sørensen, E. J. G. Peterman, T. Weber, C. F. Schmidt, and H. Flyvbjerg, Rev. Sci. Instrum. **77**, 063106 (2006).
[28] A. Rohrbach and E. H. K. Stelzer, J. Opt. Soc. Am. A **18**, 839 (2001).
[29] P. C. Ke and M. Gu, J. Mod. Opt. **45**, 2159 (1998).
[30] X. C. Yao, Z. L. Li, H. L. Guo, B. Y. Cheng, X. H. Han, and D. Z. Zhang, Chin. Phys. **9**, 824 (2000).
[31] R. Dimova, H. Polaert, and B. Pouligny, in *Scattering of Shaped Light Beams and Applications*, edited by G. Gouesbet and G. Grýhan (Research Signpost, India, 2000), p. 45, this work is available for download at http://www.mpikg.mpg.de/th/people/dimova/publications
[32] E. J. G. Peterman, F. Gittes, and C. F. Schmidt, Biophys. J. **84**, 1308 (2003).